Analytical Model of the Pantograph-Catenary Dynamic Interaction and Comparison with Numerical Simulations

J. Gil*, S. Gregori, M. Tur, F.J. Fuenmayor

Centro de Investigación en ingeniería Mecánica
Universitat Politècnica de València
Camino de Vera s/n, 46022 Valencia, Spain

Abstract

Catenaries are large cable structures which transmit electric current to trains through sliding contact with a pantograph. The Finite Element Method (FEM) is widely used to model this dynamic interaction problem and obtain the contact force between the pantograph and the catenary. As an alternative, analytical models can also be used to study catenary dynamics, although they require certain simplifications of the features considered in numerical models. In this paper, an analytical model composed of an infinite string and a visco-elastic support is introduced and enhanced by considering a Kelvin-Voigt damping model and the initial height of the contact wire. Considering the Finite Element (FE) model as a reference, the analytical model parameters are properly adjusted through static and wave propagation analyses to achieve similar behaviour in both the analytical and the FE models. To check the performance of the proposed model, the steady-state response of the pantograph-catenary coupled system is calculated and compared with the results of the FE model. Finally, the analytical model is used to analyse the interference phenomenon produced during two-pantograph operation.

*Corresponding author
Email addresses: jaigiro@upv.es (J. Gil), sangreve@upv.es (S. Gregori), m.tur@mcm.upv.es (M. Tur), ffuenmay@mcm.upv.es (F.J. Fuenmayor)

Keywords: Analytical catenary model, Pantograph dynamic interaction, Finite element, Infinite string, Pantograph interference

1. Introduction

Overhead contact lines, commonly known as railway catenaries, are currently the most widely used systems to supply high-speed trains with power through sliding contact with a moving pantograph. The dynamic behaviour of the pantograph-catenary interaction is of great interest in the system design as it can affect the reliability of vehicle operation. For this reason, many catenary models have been developed [1] and used to analyse the influence of design parameters in the current collection quality. These simulations are regulated and must be validated according to specific standards (EN50318 [2]).

Finite Element (FE) models are the most frequently used technique to simulate the problem, as shown in the recent benchmark exercise [3]. For example, in previous studies [4, 5, 6], FE-based models have been used to analyse the influence of certain design parameters in the current collection quality, which is usually quantified by the standard deviation of the interaction contact force (CF). These studies concluded that higher CF variation is obtained when the operational velocity is close to the contact wire wave velocity, when there is higher stiffness variation along the span or when the pantograph collector head has greater mass.

As an alternative to FE models, analytical catenary models are also found to be a useful tool in providing a better understanding of the role played by the design variables in exchange for adopting certain simplifications. For example, in [7], the catenary is modelled as a single and two-degrees-of-freedom system with periodically time-varying mass and stiffness and the relations between the system parameters and the upper limit of the train speed are stated. In [8] an analytical model was used to analyse the interference between pantographs when two pantographs run simultaneously in a vehicle. An optimum distance between the pantographs is theoretically calculated, based on the phase opposition of the

vertical displacement of the contact wire produced by the trailing pantograph and the displacement induced by the leading pantograph.

An infinite string with visco-elastic support is used in [9] to obtain the stationary response of lumped-parameters moving models coupled to the string. More complex infinite string models include periodic discrete elements, such as in [10] or in [11], in which a two-level infinite catenary model, composed of an upper and lower string (governed by the one-dimensional wave equation) joined by periodic supports and dampers, is simulated with a pantograph modelled by a harmonic point-load. Other similar models can be also found in the literature, such as that in [12] which is composed of several finite strings and is used to study the wave propagation and reflection phenomena in the catenary.

The objective of this paper is to propose a new analytical pantograph-catenary coupled model to obtain in a closed-form expression the pantograph interaction contact force. The proposed model is based on a previous model presented in [9]. In this work, the governing equation is modified to include a Kelvin-Voigt damping model in order to get a dissipative behaviour similar than that incorporated into the FE model. This modification implies to raise the order of the equation and the new solution is presented throughout the paper. Furthermore, the geometry of the contact wire under gravity is considered in the proposed model. The initial contact wire height profile is one of the main causes of CF variation as some studies shown [13]. Also, in [14, 15], the authors conclude that the geometric irregularities of the contact wire have a stronger influence on CF than other sources of irregularity, especially at high operating velocities as shown in [16]. This influence is also studied in [17, 18], which conclude that the optimal initial geometry significantly reduces CF variation. The analytical string models of the catenary found in the literature do not include the initial contact wire height profile and therefore, its important effect is not reflected in their results.

The interaction contact force obtained with the analytical model is compared with a verified FE model solution [19, 20]. With the aim to obtain a response as similar as possible to that of FE models, the stiffness and mass parameters of

the analytical model are properly tuned by following a proposed methodology based on static and wave propagation considerations. Finally, as an example of application of the proposed model, a new approach is raised for understanding the multiple pantograph interference, by proposing a simplified analytical expression to evaluate the optimal distances between pantographs. This problem was also studied in [21], which obtained smaller CF variation in the trailing pantograph by using an auxiliary pantograph, or in [16], which showed reduced performance when the elapsed time between the pantographs passage matches the natural catenary frequencies.

The contents of this paper are organised as follows. After this introduction, the formulation of the reference FE model is described in Section 2. The proposed analytical model is developed in Section 3 and a procedure to obtain the required parameter's values is presented in Section 4. The results obtained by the proposed model and their validation are given in Section 5, before the concluding remarks in Section 6.

2. Reference models

The Finite Element Method (FEM) is the technique most frequently used to model railway catenaries [3]. These structures are composed of different wires and bars as can be seen in Fig. 1. In this paper, the catenary FE model [19, 20] validated according to EN 50318 [2] is taken as the reference for the analytical model. The material properties and the geometric parameters of the model used are defined in the annex.

The pantograph is an articulated device on the locomotive roof that keeps in contact with the catenary. Although there are different options for modelling pantographs, in this work a lumped parameter model is used for its wide use and simplicity. The model consists of three masses that move vertically, which are connected by springs and dampers as shown in Fig. 2 (a). The pantograph lifting mechanism is replaced by a force applied on the bottom mass. For the pantograph-catenary interaction, the *penalty* method is used, which considers a

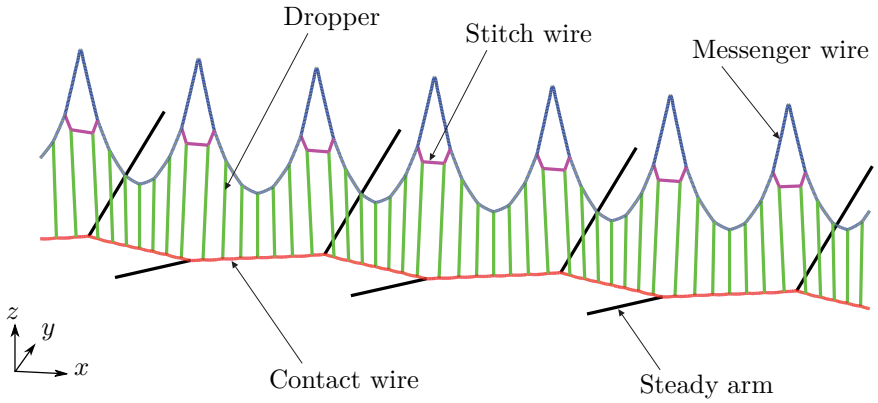

Figure 1: *FE model of the catenary.*

high stiffness element ($k_h = 50,000$ N/m [2]) placed between the contact wire and the upper mass of the pantograph as depicted in Fig. 2 (b) and exerting a contact force f_c between both models as view in Fig. 2 (c).

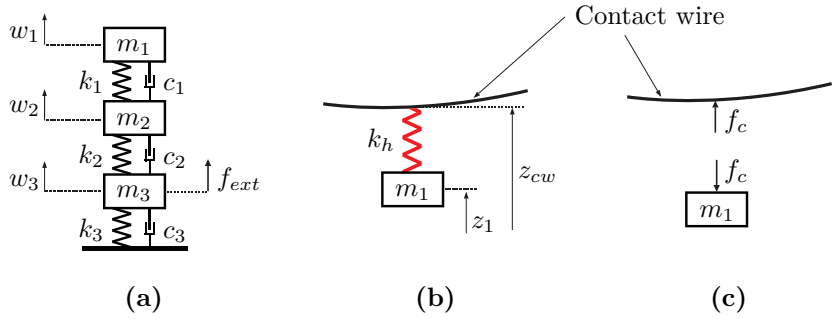

Figure 2: *(a) Pantograph model, (b) penalty model and (c) contact force* $f_c > 0$.

To obtain the initial geometry of the catenary model, the static equilibrium equation and certain design constraint equations must be solved simultaneously. The reader is referred to [19], where this problem is described in detail. Once the initial configuration of the catenary has been solved, the pantograph-catenary

dynamic interaction problem is solved by following the procedure described in [20]. This problem can be stated assuming small displacements with respect to the static equilibrium position, which means it is governed by the linear equation:

$$\mathbf{M}\ddot{\mathbf{u}} + \mathbf{C}\dot{\mathbf{u}} + \mathbf{K}\mathbf{u} = \mathbf{F} \tag{1}$$

where $\mathbf{u}$, $\dot{\mathbf{u}}$ and $\ddot{\mathbf{u}}$ are the nodal displacements, velocities and accelerations respectively. $\mathbf{K}$ and $\mathbf{M}$ are the stiffness and mass matrices and a Rayleigh damping model is used to define the damping matrix $\mathbf{C} = \alpha\mathbf{M} + \beta\mathbf{K}$ with $\alpha = 0.0125$ s^{-1} and $\beta = 10^4$ s [3]. $\mathbf{F}$ is the vector of external forces applied to the pantograph. Despite the linear appearance, this is in fact a non-linear problem, since dropper slackening and contact loss are considered in the model. The Newmark or HHT [22] schemes can be used for the numeric integration of Eq. (1) combined with an iterative method to deal with the aforementioned non-linearities.

3. Analytical model of the catenary

Here we propose an analytical catenary model based on the infinity string proposed in [9]. The model is enhanced with the introduction of a Kelvin-Voigt damping model and the consideration of the initial geometry of the contact wire. The final model proposed is used to obtain the CF produced in the pantograph-catenary dynamic interaction problem.

3.1. Initial model

For the sake of clarity, we here summarise the model presented in [9] composed of an axially loaded infinite string prestressed with a force T and supported by a continuous visco-elastic layer, as shown in Fig. 3, with $\bar{k}$ and $\bar{c}$ being the stiffness and damping coefficients per unit of length, respectively. The linear density μ can also include the influence of the mass of the support.

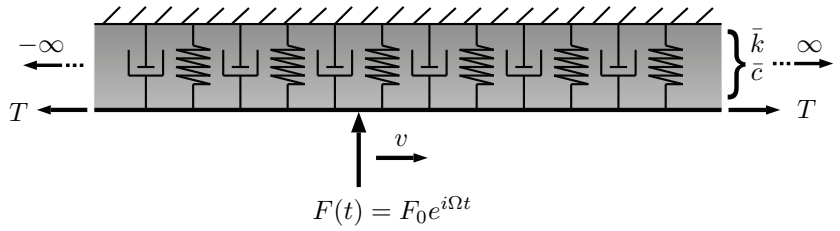

Figure 3: *Initial analytical string model (ASM1) with visco-elastic support under a harmonic moving load.*

The initial analytical string model (ASM1) subjected to a distributed load $p(x,t)$ is governed by the equation:

$$\mu \frac{\partial^2 w}{\partial t^2} - T\frac{\partial^2 w}{\partial x^2} + \bar{c}\frac{\partial w}{\partial t} + \bar{k}w = p(x,t) \tag{2}$$

where $w = w(x,t)$ is the vertical displacement of the contact wire.

The steady solution of Eq. (2) when the contact wire is loaded by a concentrated harmonic moving force $F(t) = F_0 e^{i\Omega t}$ (see Fig. 3) with frequency Ω, and velocity v, is given in [9]. In this case, the right-hand side term can be expressed as:

$$p(x,t) = F_0 e^{i\Omega t}\ \delta(x - vt) \tag{3}$$

where δ is the *Dirac* function. The solution of this problem is different for v greater or smaller than the critical velocity $v_c = \sqrt{T/\mu}$. However, as the standard EN50318 [2] limits the train velocity to $v < 0.7v_c$, the solution used in this work is that in which $v < v_c$ or equivalently $\lambda > 0$, with $\lambda = T - \mu v^2$. In this case, the expression for the string vertical displacement is:

$$w(x,t) = \begin{cases} \dfrac{iF_0 e^{-i\left[k_1^\Omega (x-vt) - \Omega t\right]}}{\lambda\left(k_2^\Omega - k_1^\Omega\right)} & if \quad x - vt > 0 \\ \dfrac{iF_0 e^{-i\left[k_2^\Omega (x-vt) - \Omega t\right]}}{\lambda\left(k_2^\Omega - k_1^\Omega\right)} & if \quad x - vt \leq 0 \end{cases} \tag{4}$$

where k_1^Ω and k_2^Ω are the poles of the system:

$$\begin{aligned} k_1^\Omega &= \left[\frac{2\mu v\Omega + p_s}{2\lambda}\right] - i\left[\frac{\bar{c}v + q_s}{2\lambda}\right] \\ k_2^\Omega &= \left[\frac{2\mu v\Omega - p_s}{2\lambda}\right] - i\left[\frac{\bar{c}v - q_s}{2\lambda}\right] \end{aligned} \tag{5}$$

being:

$$\begin{aligned} p_s &= \left[\frac{1}{2}\left(\sqrt{A^2 + B^2} + A\right)\right]^{\frac{1}{2}} \\ q_s &= \left[\frac{1}{2}\left(\sqrt{A^2 + B^2} - A\right)\right]^{\frac{1}{2}} \\ A &= 4T\mu\Omega^2 - \bar{c}^2v^2 - 4\lambda\bar{k} \\ B &= 4T\Omega\bar{c} \end{aligned} \tag{6}$$

The first expression in Eq. (4) applies to the points behind the excitation point $x - vt > 0$, while the second part is defined for the points ahead the excitation point $x - vt \leq 0$.

3.2. Simplifying assumptions in the analytical model

Important simplifications are adopted in ASM1 if compared to the more complex FE models. This simplifications also applies to the later presented ASM2.

- **Continuous support**. In the FE model, the catenary can be divided into two parts, namely, the contact wire and the set composed of droppers, steady arms and the messenger wire. In the analytical model these two parts can also be identified, but the latter is simplified by a continuous visco-elastic support which does not strictly describe the complex dynamics of the droppers and the messenger wire.

- **Constant stiffness**. Another feature accounted for in the FE model is the uneven stiffness and mass distribution of the support which holds the contact wire by discrete points (dropper connections), leading to additional irregularities and wave reflection.

- **No propagation at the support**. Furthermore, in the FE model any two different points of the support are coupled, which allows the perturbations to propagate in the support, while in the analytical model the wave propagation only occurs in the contact wire.

- **No moment of inertia**. Another simplification of the ASM1 is neglecting the bending stiffness of the contact wire.

- **Straight string**. Small displacements are considered in the initial configuration of the contact wire, thus allowing the use of a straight string dynamic equation.

- **Steady state**. As the catenary is assumed to be a long enough periodic structure, only the steady-state response is considered by ASM1.

Despite these simplifications, the analytical model includes the basic features of the catenary and leads to analytical expressions which provide explicit information on how the design parameters influence the solution.

3.3. Consideration of a Kelvin-Voigt damping model

In the catenary FE model, a proportional Rayleigh damping model is used in which the damping matrix is a linear combination of the mass and stiffness matrices ($\mathbf{C} = \alpha\mathbf{M}+\beta\mathbf{K}$). In this section, an extension of the previous analytical model is proposed with a damping model similar to that of the FE model. Following the procedure presented in [23], a Kelvin-Voigt damping model is included in the differential equation Eq. (2) by writing the damping coefficients as a linear combination of the inertial and elastic terms:

$$\mu\frac{\partial^2 w}{\partial t^2} - T\frac{\partial^2 w}{\partial x^2} + \left(\alpha\mu + \beta\bar{k}\right)\frac{\partial w}{\partial t} - \beta T\frac{\partial}{\partial t}\left(\frac{\partial^2 w}{\partial x^2}\right) + \bar{k}w = p(x,t) \qquad (7)$$

Note that in ASM1 the term $T\partial^2 w/\partial x^2$ is lacking its corresponding proportional damping term in the differential equation, which means the damping model in ASM1 is not comparable to the one in the FEM model.

This proposed analytical string model (hereinafter called ASM2) has an additional term and has become a third order equation. In the case of a moving

external force of frequency Ω, the improper integral used to compute $w(x,t)$ has a third order polynomial denominator instead of the second order polynomial in the ASM1 [9]:

$$w(x,t) = \frac{1}{2\pi}\int_{-\infty}^{\infty} \frac{F_0\ e^{-i(k(x-vt)-\Omega t)}}{\lambda k^3 + \eta k^2 + \tau k + \sigma}\mathrm{d}k \tag{8}$$

where:

$$\begin{aligned}
\lambda &= i\beta T v \\
\eta &= T - \mu v^2 + i\beta T\Omega \\
\tau &= i\left(\alpha\mu + \beta\bar{k}\right)v - 2\mu v\Omega \\
\sigma &= \bar{k} + i\left(\alpha\mu + \beta\bar{k}\right)\Omega - \mu\Omega^2
\end{aligned} \tag{9}$$

In this case the system has three poles k_1^Ω, k_2^Ω and k_3^Ω whose analytical expressions are:

$$\begin{aligned}
k_1^\Omega &= -\frac{\eta}{3\lambda} - \frac{\sqrt[3]{2}Q}{3\lambda S} + \frac{S}{3\sqrt[3]{2}\lambda} \\
k_2^\Omega &= -\frac{\eta}{3\lambda} - \left(-\frac{1}{2} + \frac{i\sqrt{3}}{2}\right)\frac{\sqrt[3]{2}Q}{3\lambda S} + \left(-\frac{1}{2} - \frac{i\sqrt{3}}{2}\right)\frac{S}{3\sqrt[3]{2}\lambda} \\
k_3^\Omega &= -\frac{\eta}{3\lambda} - \left(-\frac{1}{2} - \frac{i\sqrt{3}}{2}\right)\frac{\sqrt[3]{2}Q}{3\lambda S} + \left(-\frac{1}{2} + \frac{i\sqrt{3}}{2}\right)\frac{S}{3\sqrt[3]{2}\lambda}
\end{aligned} \tag{10}$$

where:

$$\begin{aligned}
S &= \sqrt[3]{R + \sqrt{4Q^3 + R^2}} \\
Q &= 3\lambda\tau - \eta^2 \\
R &= -2\eta^3 + 9\eta\lambda\tau - 27\lambda^2\sigma
\end{aligned} \tag{11}$$

Applying the residue theorem to Eq. (8), the string vertical displacement is:

$$w(x,t) = \begin{cases}
iF_0 \displaystyle\sum_p \frac{e^{-i\left(k_p^\Omega(x-vt)-\Omega t\right)}}{\lambda \displaystyle\prod_{r\neq p}\left(k_p^\Omega - k_r^\Omega\right)}; & x - vt \leq 0 \\
-iF_0 \displaystyle\sum_q \frac{e^{-i\left(k_q^\Omega(x-vt)-\Omega t\right)}}{\lambda \displaystyle\prod_{r\neq q}\left(k_q^\Omega - k_r^\Omega\right)}; & x - vt > 0
\end{cases} \tag{12}$$

where k_p^Ω are the poles with a positive imaginary part and k_q^Ω are the poles with a negative imaginary part. As in the ASM1, the solution is divided into two

expressions which correspond to the displacements of the string section behind and ahead of the load application point, respectively. Each part of the solution consists of a sum of exponential terms which represent damped waves. In ASM2 there are three terms (or waves) included in the solution corresponding to the three poles. The poles with a positive imaginary part are contained in the first part of the solution, where $x - vt \leq 0$, while the poles with a negative imaginary part are used in the expression valid for $x - vt > 0$.

In the simpler ASM1 model, the sign of the imaginary part of the two poles depends on the velocity v. If $v < v_c$, there is one pole with a negative imaginary part and one pole with a positive imaginary part, which corresponds to a backward and a forward wave, respectively. On the other hand, if $v > v_c$, both poles have positive imaginary parts and the two waves propagate backwards, the section ahead of the applied force remaining unaltered. In the ASM2 it is difficult to find a mathematical criterion to define the sign of the imaginary part of the poles. However, numerical tests reveal that the imaginary parts of the poles do not vary their signs in the range of interest of Ω and v, if the values of the parameters T, $\bar{k}$ and μ are those obtained in Section 4. Specifically, only one pole k_1^Ω has a negative imaginary part, while the other two poles k_2^Ω and k_3^Ω remain with a positive imaginary part.

To highlight this feature, in Fig. 4 the imaginary part of the poles of ASM2 is plotted versus the velocity v for the excitation frequency $\Omega = 10$ Hz. It is important to note that this behaviour is analogous for all the frequencies studied and although the imaginary part of the poles is very close to zero for some values of v, it does not actually reach that value in any case. In ASM2 there is no critical speed at which the signs of the poles change, however, the solution is similar to that of ASM1. For speeds below v_c of ASM1 ($\sim$146 m/s with the parameter used in this paper) the imaginary part of k_3^Ω is very large and its associated wave is strongly damped. Thus, the only noticeable waves are those related to the poles k_1^Ω and k_2^Ω, as in ASM1. The same explanation is applicable for speeds greater than v_c, in which the absolute value of the imaginary part of k_1^Ω is large enough and for that reason has a negligible influence. In this case, k_2^Ω,

k_3^Ω are the dominant poles and there are two noticeable backward waves, as in ASM1. Despite these similarities, the damping is different in the two analytical models and the influence of the additional pole in ASM2 is considerable for velocities close to v_c and also for points close to the load point.

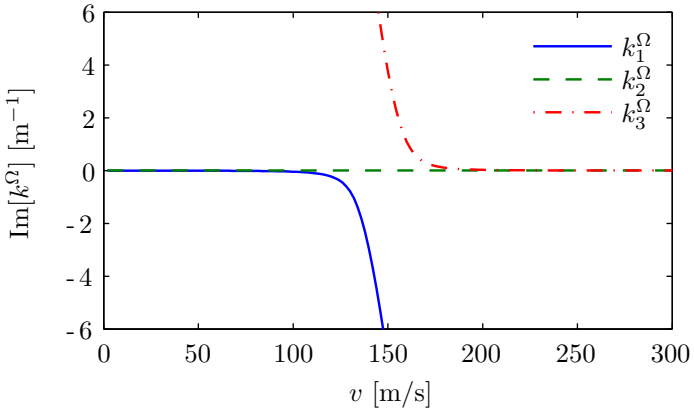

Figure 4: *Imaginary part of the poles of the ASM2 respect to v for $\Omega = 10$ Hz.*

3.4. Model with contact wire initial geometry and pantograph coupling

The force of gravity produces an uneven initial height of the contact wire, which is properly considered in the FE model. In this section, a realistic contact wire initial height profile is included in ASM2. For this, the total string height can be written as:

$$z(x,t) = z_0(x) + w(x,t) \tag{13}$$

where $z_0(x)$ is the initial height, which depends on the position x and, $w(x,t)$ satisfies Eq. (7) thanks to the linearity of the problem.

As catenaries can generally be assumed as periodic structures composed of a succession of equal spans, the height of the contact wire is a periodic function that can be broken down into a sum of harmonic functions by means of the Fourier transform. Due to the linearity of the system, the problem can be solved first by considering a harmonic height $z_0(x)$, after which the superposition principle can be applied to get the solution with a general contact wire height in a further step.

The objective is to solve the dynamic interaction of two pantographs coupled to ASM2, which now incorporates an initial harmonic height $z_0(x)$. The pantographs move at the same speed v and are separated by a distance L, as seen in Fig. 5.

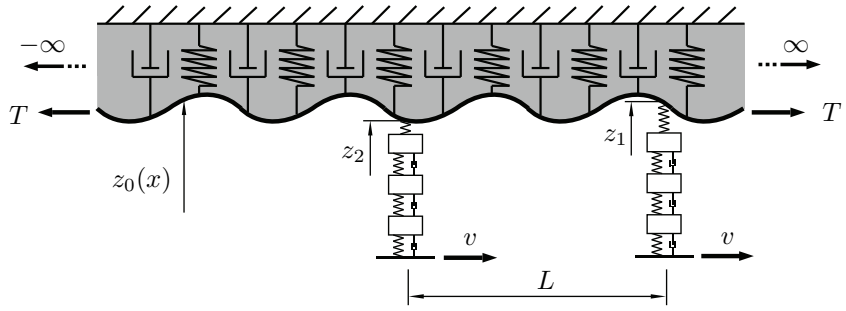

Figure 5: *Two pantographs coupled to the ASM2 with initial height $z_0(x)$.*

The methodology followed in [9] consists of using the dynamic stiffness matrices to solve the coupled interaction between the string and the pantograph models. In this paper the same methodology is considered to solve the problem, but nevertheless, the receptance functions are used and only one degree of freedom is included per pantograph, which corresponds to the vertical displacement of the point in contact with the string. The problem is thus reduced in size without affecting the accuracy of the results. Furthermore, in the case of two pantographs, this simplification can obtain an analytical expression of the solution.

In order to apply the described procedure, it is first necessary to obtain the Frequency Response Function (FRF). Given two points 1 and 2 on the string, located at a distance L and both moving at the same speed v (see Fig. 6), the FRF of the string H_{12} is defined as the ratio between the vertical displacement of 1 and the harmonic force applied at 2:

$$H_{12}(\Omega) = \frac{w(vt + L, t)}{F_0 e^{i\Omega t}} \tag{14}$$

Replacing the expression (4) in Eq. (14) and considering the signs of the imag-

inary parts of the poles discussed previously (Sec. 3.3), the FRF is:

$$H_{12}(\Omega) = \frac{-ie^{-ik_1^\Omega L}}{\lambda\left(k_1^\Omega - k_2^\Omega\right)\left(k_1^\Omega - k_3^\Omega\right)} \tag{15}$$

Similarly, H_{21} can be defined as the ratio between the displacement produced in 2 and the excitation applied at 1:

$$H_{21}(\Omega) = \frac{ie^{ik_2^\Omega L}}{\lambda\left(k_2^\Omega - k_1^\Omega\right)\left(k_2^\Omega - k_3^\Omega\right)} + \frac{ie^{ik_3^\Omega L}}{\lambda\left(k_3^\Omega - k_1^\Omega\right)\left(k_3^\Omega - k_2^\Omega\right)} \tag{16}$$

When the displacement is measured at the force application point, the direct FRF is:

$$H_{11}(\Omega) = H_{22}(\Omega) = \frac{-i}{\lambda\left(k_1^\Omega - k_2^\Omega\right)\left(k_1^\Omega - k_3^\Omega\right)} \tag{17}$$

It is also necessary to calculate the FRF of the pantograph model, which includes a penalty stiffness k_h on the upper mass (see Fig. 2). The pantograph FRF is thus defined as the ratio between the displacement of the upper point ($1'$ or $2'$ in Fig. 6) and the harmonic force applied at the same point:

$$H_p(\Omega) = \frac{1}{k_h} + \left[-\Omega^2\mathbf{M}_p + i\Omega\mathbf{C}_p + \mathbf{K}_p\right]^{-1}_{(1,1)} \tag{18}$$

where $\mathbf{M}_p$, $\mathbf{C}_p$ y $\mathbf{K}_p$ are the mass, damping and stiffness matrices of the pantograph respectively, and the operator $[\ ]_{(1,1)}$ extracts the first row and first column element of the matrix which refers to the upper mass degree of freedom.

The contact forces F_1 and F_2 between each pantograph and the string, represented in Fig. 6, are the unknowns of the problem. The linearity of Eq. (7) allows writing the vertical displacement of the points 1 and 2 as the superposition of the displacement produced by each force acting separately. The height of points 1 and 2 are thus the sum of the initial height of the contact wire and the displacement produced by the contact forces according to the scheme in Fig. 6. This is:

$$\begin{aligned} z_1(t) &= z_{01}(t) + H_{11}(\Omega)F_1(t) + H_{12}(\Omega)F_2(t) \\ z_2(t) &= z_{02}(t) + H_{21}(\Omega)F_1(t) + H_{22}(\Omega)F_2(t) \end{aligned} \tag{19}$$

where $z_{01}(t) = z_0(vt + L)$ and $z_{02}(t) = z_0(vt)$. In turn, the height of the points $1'$ y $2'$ which belong to the pantograph model are:

$$\begin{aligned} z_{1'}(t) &= -H_p(\Omega)F_1(t) \\ z_{2'}(t) &= -H_p(\Omega)F_2(t) \end{aligned} \tag{20}$$

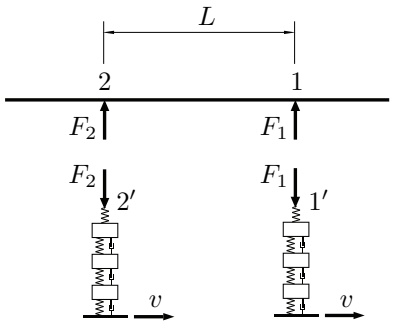

Figure 6: *Contact forces in the coupled string model with two pantographs.*

Since the initial height is considered a harmonic function of frequency Ω, it is possible to write them as:

$$\begin{aligned} z_{01}(t) &= \tilde{z}_{01} e^{i\Omega t} \\ z_{02}(t) &= \tilde{z}_{02} e^{i\Omega t} \end{aligned} \tag{21}$$

in which, there is a phase shift between the phasors $\tilde{z}_{01}$ and $\tilde{z}_{02}$

$$\tilde{z}_{01} = \tilde{z}_{02} e^{i\frac{\Omega L}{v}} \tag{22}$$

due to the distance between the points. This phasor notation can also be used for the CFs:

$$\begin{aligned} F_1(t) &= \tilde{F}_1 e^{i\Omega t} \\ F_2(t) &= \tilde{F}_2 e^{i\Omega t} \end{aligned} \tag{23}$$

Since the points 1 and 2 match with the points $1'$ and $2'$, the left hand side terms of Eqs. (19) and (20) can be equated to obtain the following system of equations:

$$\begin{bmatrix} -H_p(\Omega) - H_{11}(\Omega) & -H_{12}(\Omega) \\ -H_{21}(\Omega) & -H_p(\Omega) - H_{22}(\Omega) \end{bmatrix} \begin{Bmatrix} \tilde{F}_1 \\ \tilde{F}_2 \end{Bmatrix} = \begin{Bmatrix} \tilde{z}_{01} \\ \tilde{z}_{02} \end{Bmatrix} \tag{24}$$

which can be arranged in matrix notation:

$$\mathbf{H}(\Omega)\ \tilde{\mathbf{F}} = \tilde{\mathbf{z}}_0 \tag{25}$$

As stated above, in the static equilibrium configuration, the catenary contact wire adopts a periodic height $z_0(x)$ whose period is equal to the span length L_v.

The periodic function $z_0(x)$ can be represented by the Fourier series:

$$z_0(x) = Z_0 + \sum_{n=1}^{\infty} Z_n \; e^{ik_n x} \tag{26}$$

where Z_0 is the mean value of the function, Z_n are the complex Fourier coefficients and the wavenumber is:

$$k_n = \frac{2\pi n}{L_v} \qquad \text{for} \qquad n \in \mathbb{N} \tag{27}$$

By solving Eq. 25, the contact force of two pantographs coupled to ASM2 are obtained for the case of an initial harmonic height. Since that system is linear, the more general case in which $z_0(x)$ is a periodic function can also be solved by applying Eq. (26) and the superposition principle:

$$\mathbf{F}(t) = \mathbf{F}_m + \sum_{n=1}^{\infty} \mathbf{H}^{-1}(\Omega_n) \; \tilde{\mathbf{z}}_{0,n} \; e^{i\Omega_n t} \tag{28}$$

where $\mathbf{F}_m$ is the vector with the mean CF of every pantograph, the excitation frequency is:

$$\Omega_n = k_n v \tag{29}$$

and $\tilde{\mathbf{z}}_{0,n}$ groups the complex Fourier coefficients of the contact wire initial height, which considers the phase shift between the pantographs:

$$\tilde{\mathbf{z}}_{0,n} = \left\{ \begin{array}{c} Z_n e^{i\frac{\Omega_n L}{v}} \\ Z_n \end{array} \right\} \tag{30}$$

4. Parameter setting

This section is devoted to determining the ASM2 parameters required to achieve similar behaviour to the reference FE model. These include: string tension T, support stiffness $\bar{k}$ and linear density μ. The α and β damping parameters are the same as those considered in the FE model. The tension T can be taken directly from the FE model. This is given by the value of the axial pretension of the contact wire, which is 31500 N in this study.

4.1. Setting visco-elastic support stiffness

The value of $\bar{k}$ is tuned by comparing the static equilibrium response in both the ASM2 and FE models. Given a vertical force applied at a certain point on the contact wire, the vertical stiffness k_z is defined as the ratio between the applied force and the vertical displacement at the application point. This parameter is constant at any point in ASM2. However, as the FE model is not homogeneous and k_z varies according to the position in the span, as shown in Fig. 7, its mean value $k_{z,\mathrm{FEM}} = 2538.7$ N/m is adopted as a representative value.

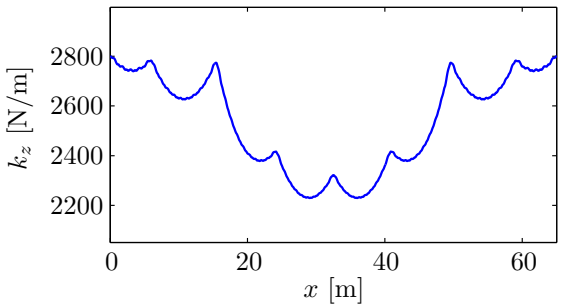

Figure 7: *Vertical stiffness k_z of the contact wire of the FE model in a span.*

Vertical stiffness k_z can be calculated in ASM2 by using the direct FRF defined in Eq. (17), assuming $v = 0$ and $\Omega = 0$:

$$k_z = H_{11}^{-1}\Big|_{\substack{\Omega=0\\ v=0}} = 2\sqrt{\bar{k}\,T} \tag{31}$$

Thus, if k_z is enforced to match $k_{z,\mathrm{FEM}}$:

$$\bar{k} = \frac{k_{z,\mathrm{FEM}}^2}{4\,T} \tag{32}$$

which leads to a visco-elastic support stiffness $\bar{k} = 51.15$ N/m^2.

In order to check the static solution with the adjusted $\bar{k}$, the FE model and ASM2 are compared in Fig. 8, in which the vertical displacement of the contact wire is adimensionalised with respect to its value at the load application point.

Two curves are shown for the FE model, in which the load is applied in the middle of the span and in the steady arm. There is clearly good agreement between the response of both models, especially when the force is applied on the steady arm.

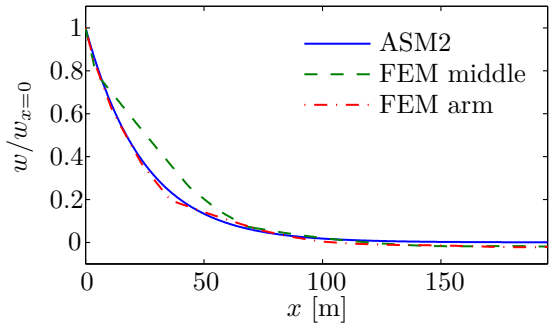

Figure 8: *Adimensionalised displacement of the contact wire in FE model and ASM2 produced by a static force.*

4.2. Setting string linear density

To obtain string linear density μ, is not enough to consider only the mass of the catenary contact wire, the mass of the other parts of the catenary must also be taken into account. A wave propagation analysis is performed to adjust the value of μ, so that similar behaviour is found in ASM2 and the FE model. For this, the response of the contact wire is calculated in both models for a harmonic force with $v = 0$.

In this scenario, as the load has no forward velocity there are only two poles, k_1^Ω and k_2^Ω, in ASM2 and the displacement of the contact wire (backward side) is given by:

$$w(x,t) = \frac{ie^{-i\left(k_2^\Omega x - \Omega t\right)}}{\eta\left(k_2^\Omega - k_1^\Omega\right)} \tag{33}$$

where $\eta = T + i\beta T\Omega$ and the poles are:

$$\begin{aligned} k_1^\Omega &= \left[\frac{p_s}{\sqrt{T+\beta^2 T\Omega^2}}\right] - i\left[\frac{q_s}{\sqrt{T+\beta^2 T\Omega^2}}\right] \\ k_2^\Omega &= \left[\frac{-p_s}{\sqrt{T+\beta^2 T\Omega^2}}\right] + i\left[\frac{q_s}{\sqrt{T+\beta^2 T\Omega^2}}\right] \end{aligned} \tag{34}$$

in which, q_s and p_s are those defined in Eq. (6), but now the coefficients A and B are:

$$A = -\bar{k} - \beta\left(\alpha\mu + \beta\bar{k}\right)\Omega^2 + \mu\Omega^2$$
$$B = \left(\alpha\mu + \beta\bar{k}\right)\Omega - \beta\bar{k}\Omega + \beta\mu\Omega^3 \tag{35}$$

Eq. (33) represents a damped wave whose wavelength is:

$$\lambda_\Omega = -\frac{2\pi}{k_{2R}^\Omega} \tag{36}$$

k_{2R}^Ω being the real part of k_2^Ω. This wavelength λ_Ω is very sensitive to μ, as can be seen in Fig. 9, in which λ_Ω is plotted for different values of the excitation frequency and μ. λ_Ω is therefore a suitable magnitude to adjust linear density μ.

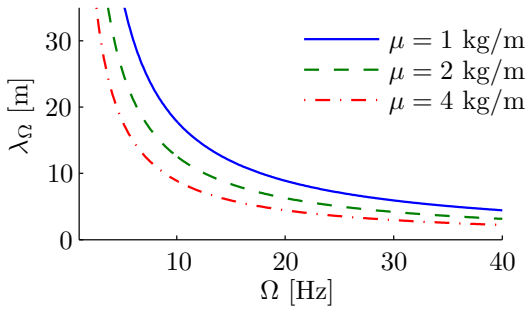

Figure 9: *Wavelength λ_Ω of ASM2 with $v = 0$.*

The same problem is solved for the FE model. Assuming linear behaviour of the FE catenary model (see Eq. (1)), the steady response when it is loaded by a harmonic external force with frequency Ω is:

$$\mathbf{u}(t) = \left[\left(-\Omega^2\mathbf{M} + i\Omega\mathbf{C} + \mathbf{K}\right)^{-1}\hat{\mathbf{F}}e^{i\Omega t}\right]_{Re} \tag{37}$$

where $\hat{\mathbf{F}}$ is a vertical unit force applied to the contact wire at the middle of the span. The particular solution $\mathbf{u}(t)$ of Eq. (37) leads to a contact wire vertical displacement function $w_{\text{FEM}}(x,t)$. If the FE model response is similar to that of ASM2, a wave with wavelength $\lambda_{\Omega_{\text{FEM}}}$ could be identified in the function

$w_{\text{FEM}}(x,t)$, for which this function is evaluated at discrete points at a certain time (for example $t = 0$):

$$w(n) = w_{\text{FEM}}(x_n, 0) \; ; \qquad x_n = (n-1)\Delta x \qquad n \in \mathbb{N} \tag{38}$$

Δx being the distance between two consecutive discrete points x_n.

The presence of a single harmonic wave in $w(n)$ cannot be guaranteed due to the complexity of the FE model, it is therefore necessary to obtain the most representative wavelength in the FE model response for every excitation frequency Ω. For this, the Fourier transform of $w(n)$ is first obtained and then the spatial frequency $k = 2\pi/\lambda$ of the Fourier term with the highest weight is found. To avoid the leakage error, the Fourier transform of $w(n)$ is carried out by a variable window whose size, N, depends on the spatial frequency. Thus, for a given k, the N used to calculate every Fourier term is forced to include M complete cycles of this spatial frequency, so that the relation between the window size and the wavelength is:

$$N(\lambda) = \frac{M\lambda}{\Delta x} \in \mathbb{N} \tag{39}$$

In this paper, the value $M = 7$ is adopted because it provides a good balance between precision and window size. For every excitation frequency Ω, the terms of the single-sided Discrete Fourier Transform (DFT) of $w(n)$ are obtained with:

$$W_\lambda(\lambda) = \frac{2}{N(\lambda)} \sum_{n=1}^{N(\lambda)} w(n)\; e^{\frac{-2\pi i M}{N(\lambda)}(n-1)} \tag{40}$$

Finally, the value of λ which produces the maximum W_λ is taken as the most representative wavelength $\lambda_{\Omega_{\text{FEM}}}$ for frequency Ω. To illustrate this method $W_\lambda(\lambda)$ for $\Omega = 10$ Hz is represented in Fig. 10, in which the maximum value is found for $\lambda_{\Omega_{\text{FEM}}} = 14.52$ m.

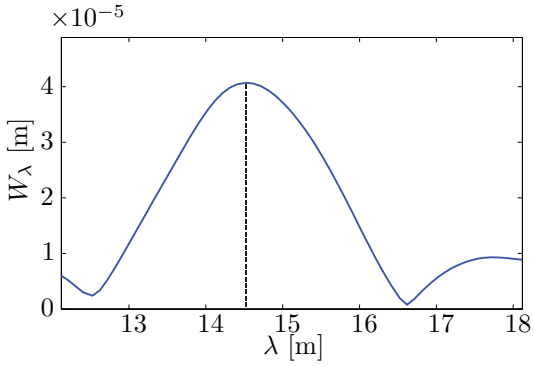

Figure 10: *DFT of $w(n)$ with variable window size with respect to the corresponding wavelength λ for $\Omega = 10$ Hz.*

The values of $\lambda_{\Omega_{\text{FEM}}}$ are obtained for excitation frequencies ranging from 10 to 40 Hz. Lower frequencies lead to very a large wavelength and the upper limit is high enough, considering the low-pass cutoff frequency of 20 Hz defined in the standard [24] for the CF. Finally, the parameter μ is obtained by a least squares fitting of λ_Ω (Eq. (36)) to the results of the FE model $\lambda_{\Omega_{\text{FEM}}} = \arg\max W_\lambda(\lambda)$. This fitting gives a value of $\mu = 1.4735$ kg/m. The good agreement between the FE model ant the fitted ASM2 wavelengths can be seen in Fig. 11.

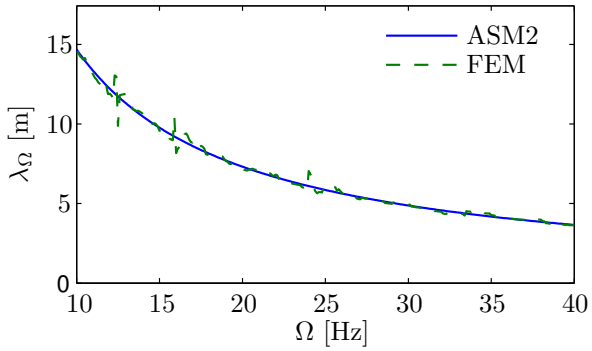

Figure 11: *Wavelength λ_Ω produced by a harmonic force in both ASM2 and the FE model.*

Two additional ranges of Ω are considered to ensure that the value of μ

obtained does not depend on the choice of this range. The μ obtained after the fitting are compared in Table 1 for the three ranges of Ω. Given the small difference between the obtained values, the fitting can be considered valid.

Table 1: *Fitted values of μ for different ranges of Ω.*

Ω [Hz]	**5-20**	**10-20**	**10-40**
μ [kg/m]	1.4652	1.4790	1.4735

5. Numerical results

In this section, ASM2 and the FE model are used to obtain and compare the contact force (CF) and its standard deviation (σ) of the pantograph-catenary dynamic interaction in different examples, considering one pantograph (single operation) and two pantographs (double operation).

The mean value of the CF, F_m, is controlled by the external force applied to the pantograph mechanism. According to the standard [24], this magnitude must fulfil the following limitation:

$$F_m \leq 0.0097v^2 + 70 \tag{41}$$

where v is the velocity of the pantograph expressed in km/h. In the ASM2 the CF is obtained as a sum of independent harmonic terms, so the mean value of the CF (F_m) does not influence either the harmonics $\tilde{F}(\Omega_n)$ or σ. On the other hand, in the FE model a higher value of F_m leads to a higher CF variation due to the uneven distribution of mass and stiffness along the contact wire. In the simulations carried out in the following examples, the maximum value of F_m according to Eq. (41) is used, since this is the case with the most CF variation. The CF is filtered by a 20 Hz low-pass filter, following the guidelines in [24].

5.1. Initial geometry of the catenary

The FE model of the catenary used in this paper is composed of periodic 65 m long spans with 7 droppers. The FEM static solution is used to determine the

height of the contact wire under the force of gravity (shown in Fig. 12), which is used to calculate the CF in the analytical model. Fig. 13 represents the spatial frequency content of the contact wire height, which allows us to express $z_0(x)$ as a sum of harmonic functions. The 7^{th} and 8^{th} harmonics depicted in Fig. 13 are the most important and are directly related to the dropper-pass frequency.

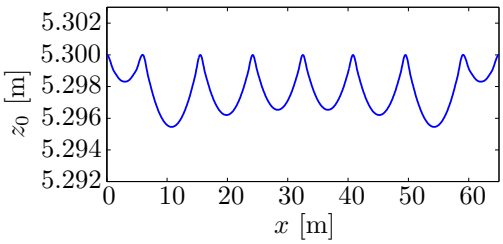

Figure 12: *Catenary contact wire height profile along a span.*

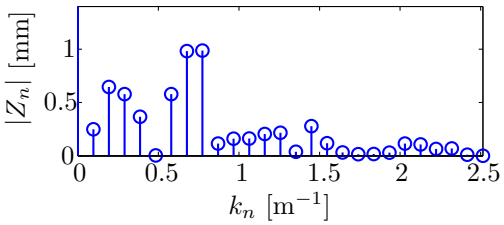

Figure 13: *Discrete Fourier Transform of the catenary contact wire height.*

5.2. Single operation

In this case, Eq. (24) can be particularised for only a single pantograph, assuming $\tilde{F}_2 = 0$:

$$-\left[H_p(\Omega) + H_{11}(\Omega)\right]\tilde{F}_n = Z_n \tag{42}$$

whose solution is:

$$\tilde{F}_n = K_D(\Omega) Z_n \tag{43}$$

the dynamic stiffness being:

$$K_D(\Omega) = \frac{\lambda(k_1^\Omega - k_2^\Omega)(k_1^\Omega - k_3^\Omega)}{i - H_p\lambda(k_1^\Omega - k_2^\Omega)(k_1^\Omega - k_3^\Omega)} \tag{44}$$

where Z_n are the Fourier terms of the initial contact wire height represented in Fig. 13.

The frequency content of the CF $\left|\tilde{F}_n(\Omega)\right|$ obtained by ASM2 is compared in Fig. 14 with that computed by the FE model for excitation frequencies ranging from 0 to 20 Hz and the pantograph running at 200, 250, 300 and 350 km/h. Note that the number of harmonics included in the considered frequency range is lower for high speeds due to the relation given in Eq. (29). There is a reasonable similarity between the results of both models since the magnitude of the analytical results is not too far from the FE results. However, great discrepancies are found at 350 km/h in the first two harmonics. They are caused probably by the high F_m imposed according to Eq. (41), since the higher the F_m the higher the influence of the stiffness variation in the FE model, which is dominated by the first harmonics.

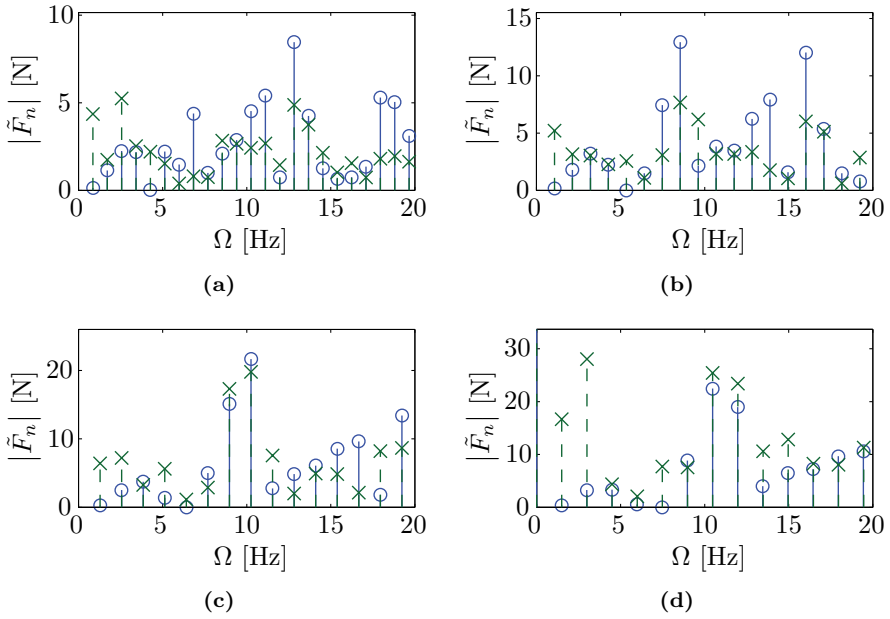

Figure 14: *CF in the frequency domain at (a) 200 km/h, (b) 250 km/h, (c) 300 km/h and (d) 350 km/h.* ○ *ASM2* × *FEM.*

The 20 Hz low-pass filtered CF is represented in the time domain in Fig. 15.

Again, although the curves do not fit perfectly, a general similarity between ASM2 and the FEM curves can be appreciated. The discrepancies found at 350 km/h are also present in this temporal representation.

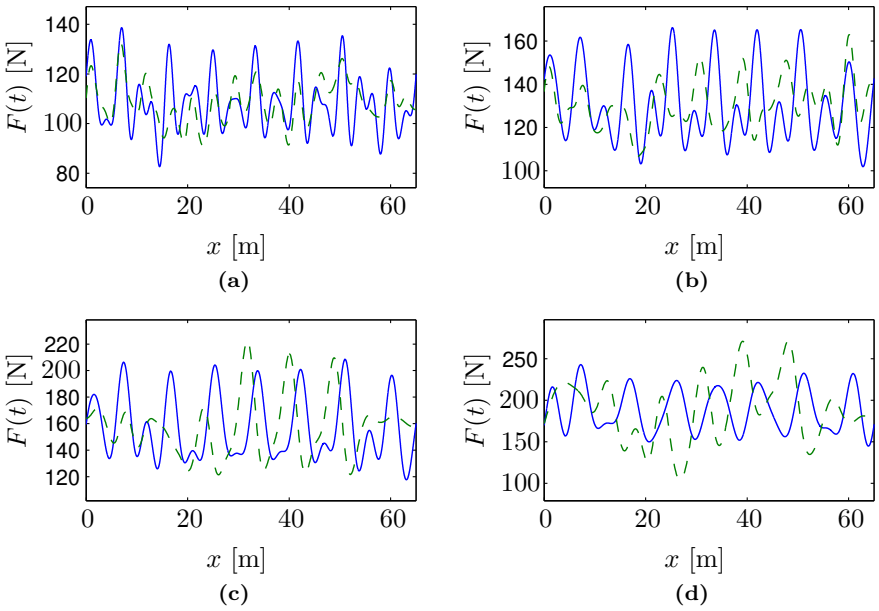

Figure 15: *CF in the time domain at (a) 200 km/h, (b) 250 km/h, (c) 300 km/h and (d) 350 km/h.* —*ASM2* - - *FEM.*

The CF standard deviation σ is the variable most often used to quantify current collection quality. σ can be computed from the CF defined in the frequency domain as:

$$\sigma = \sqrt{\frac{1}{2}\sum_{n=1}^{N_{20}} \left|\tilde{F}_n(\Omega_n)\right|^2} \tag{45}$$

where N_{20} is the number of harmonics whose frequency Ω_n is lower than 20 Hz. The standard deviation σ is plotted versus train velocity in Fig. 16. As σ depends on the mean CF in the FE model, FEM results are shown with a mean CF of 70, 80, 90 and 100% of the maximum mean CF allowed by Eq. (41). Despite all the simplifications introduced in the analytical model, it is able to give a good approximation of σ with respect to the more accurate results obtained from the

FE model. Especially, the similarity for the maximum mean contact force allowed by the standard is remarkable. Note that the mean CF effect is negligible for velocities smaller than 250 km/h for the studied pantograph-catenary system. In conclusion, the standard deviation calculated with the analytical model shows that the irregularities in contact wire height have a strong influence on the CF fluctuations.

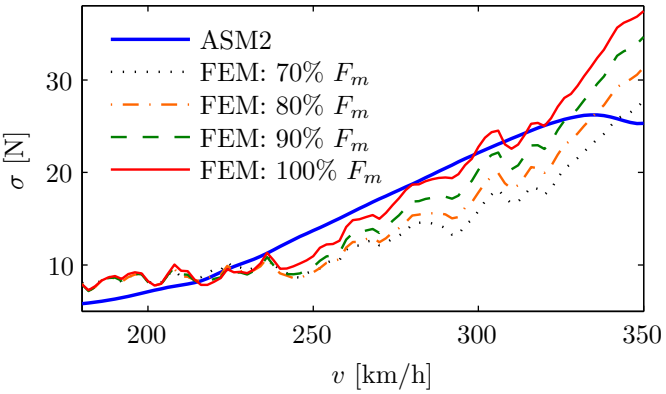

Figure 16: *Comparison of the standard deviation of the CF between the ASM2 and the FE model for different pantograph velocities and different values of the mean CF.*

5.3. Pantograph interference

In a double operation pantograph-catenary dynamic interaction, both CF pantographs affect each other. However, the interference of the leading pantograph on the trailing pantograph is much greater than in the opposite case. In this section, the trailing pantograph CF is analysed with respect to the pantographs separation distance L. To simplify the analysis, the initial height of the contact wire $z_0(x)$ is considered as a pure harmonic function with frequency Ω.

The CF of both pantographs is obtained by solving Eq. (24). The amplitude of the trailing pantograph CF reaches minimum for some L values when the displacement produced by the leading pantograph reaches the trailing pantograph in phase opposition to the given contact wire height. As obtaining an analytical

expression for the minimum values of L is rather troublesome, an approximate analytical solution is proposed below.

As the trailing pantograph has a negligible effect on the leading pantograph [8, 21], it is assumed here that $H_{12}(\Omega) = 0$, which implies that the CF of the leading pantograph is not modified with respect to the single operation scenario. With this assumption, the solution of Eq. (24) is:

$$\tilde{F}_2 = -\frac{\tilde{z}_0}{H_p + H_{22}(\Omega)} \left(1 - C_a e^{iL\left(\Omega/v + k_2^\Omega\right)} - C_b e^{iL\left(\Omega/v + k_3^\Omega\right)}\right) \tag{46}$$

where:

$$\begin{aligned} C_a &= \frac{i}{\left(H_p + H_{11}\left(\Omega\right)\right) \lambda \left(k_2^\Omega - k_1^\Omega\right) \left(k_2^\Omega - k_3^\Omega\right)} \\ C_b &= \frac{i}{\left(H_p + H_{11}\left(\Omega\right)\right) \lambda \left(k_3^\Omega - k_1^\Omega\right) \left(k_3^\Omega - k_2^\Omega\right)} \end{aligned} \tag{47}$$

Deriving the amplitude of $\tilde{F}_2$ to get the L in which it is minimum still leads to a complex expression and therefore two additional simplifications can be further introduced:

- The exponential term which includes k_3^Ω is not considered due to this wave is strongly damped for velocities lower than v_c (see Fig. 4).
- As the damping of the remaining exponential term which includes k_2^Ω is very small, $k_{2I}^\Omega = 0$ is assumed so that the position of the minima are obtained assuming a non-damped wave.

With these hypotheses, the minima of $\left|\tilde{F}_2\right|$ are found when:

$$\arg\left(C_a e^{iL\left(\Omega/v + k_{2R}^\Omega\right)}\right) = 2\pi n \; ; \qquad n = 0, 1, 2, ... \tag{48}$$

so, for every Ω there is a group of equidistant optimal values of L:

$$L_{min} = \frac{2\pi n - arg(C_a)}{\Omega/v + k_{2R}^\Omega} \tag{49}$$

For ASM2, the exact value of $\left|\tilde{F}_2\right|$ (see Eq. (25)) and the approximation given in Eq. (46), which assumes negligible interference on the leading pantograph, are compared In Fig. 17 for $\Omega = 10$ Hz and $v = 300$ km/h. The similarity

between the two curves is greater for higher L and for L close to the minima, since the hypothesis assumed is more accurate (minor influence of the trailing on the leading pantograph), while the minima of both curves are close to the values given by the approximate expression of Eq. (49). In short, for every excitation frequency Ω there are equidistant distances L_{min} for which the CF amplitude of the trailing pantograph is minimised.

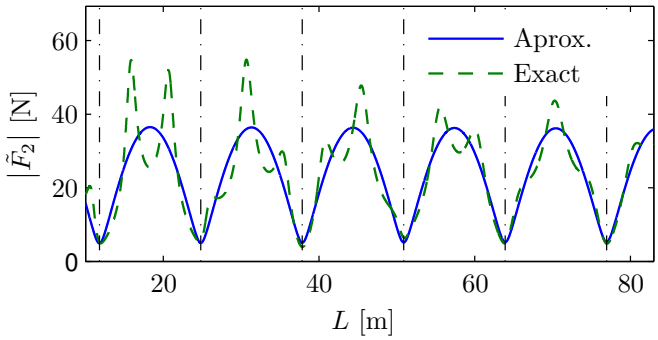

Figure 17: *Variation of approximate and exact analytical CF amplitude of the trailing pantograph with harmonic contact wire initial height of* $\Omega = 10$ *Hz, versus pantograph separation* L*, at* $v = 300$ *km/h. The* L_{min} *values given by Eq.* (49) *are represented by vertical dash-dotted lines.*

The optimal behaviour of the trailing pantograph is produced by the synchronisation of the wave generated by the leading pantograph. This physical mechanism is explained hereunder. The CF phase of the leading pantograph in single operation $\tilde{F}_1$ is taken as a reference. This force generates a wave whose vertical displacement at point 1 (see Fig. 6), considering only the part due to k_2^Ω is:

$$\tilde{w}_1 = H_{11}^{k2} \tilde{F}_1 \tag{50}$$

where:

$$H_{11}^{k2} = \frac{i}{\lambda \left(k_2^\Omega - k_1^\Omega\right)\left(k_2^\Omega - k_3^\Omega\right)} \tag{51}$$

The phase of this displacement is $\varphi_{w_1} = \arg(H_{11}^{k2})$. This wave of wavelength k_{2R}^Ω at point 2 generates a displacement with phase $\varphi_{w_2} = \varphi_{w_1} + k_{2R}^\Omega L$ due to the

distance between points 1 and 2. This displacement generates an interference force $\tilde{F}_{2i}$ on the trailing pantograph whose phase is $\varphi_{F_{2i}} = \varphi_{w_2} + \arg(K_D)$, according to Eq (43). On the other hand, the CF of the trailing pantograph in single operation $\tilde{F}_2$ has a different phase with respect to the leading pantograph CF due to the delay between both pantographs, so that $\varphi_{F_2} = -\Omega L/v$. The CF of the trailing pantograph therefore has a minimum amplitude when its force in single operation is in phase opposition with the interference force, i.e. $\varphi_{F_2^i} - \varphi_{F_2} = \pi + 2\pi n$, which is equivalent to Eq. (48) and after replacing terms reads:

$$\arg(H_{11}^{k2}) + \arg(K_D) + k_{2R}^{\Omega} L + \frac{\Omega L}{v} = \pi + 2\pi n \; ; \quad n = 0, 1, 2, ... \tag{52}$$

To conclude this section the phases mentioned above are summarised in Table 2.

Table 2: *Summary of the different phases of the magnitudes involved in the pantograph interference.*

	φ	
Pantograph/point	1	2
CF in single operation	0	$-\frac{\Omega L}{v}$
Wave produced by pant. 1	$\arg(H_{11}^{k2})$	$\arg(H_{11}^{k2}) + k_{2R}^{\Omega} L$
Interference force	——	$\arg(H_{11}^{k2}) + k_{2R}^{\Omega} L + \arg(K_D)$

5.4. Double pantograph operation

To verify the accuracy of ASM2 in double pantograph operation the σ_2 obtained is compared with the FEM results for a wide range of L at the operating speeds of 200, 250, 300 and 350 km/h (see Fig. 18). In this case, since $z_0(x)$ contains several harmonics (see Fig. 13) the fluctuating σ_2 behaviour versus changes in L is produced by the contributions of all the CF harmonics, which fluctuate every $L_{min}(\Omega)$. Considering all the differences between the models, the approximation obtained by the analytical model is reasonably good, especially

at 300 km/h. Note that the σ_2 obtained from the FE model is higher with respect to the analytical values when v increases due probably to the effect of the greater mean CF imposed, according to Eq. (41). In fact, a higher value of σ_2 at 350 km/h in the FEM model was already given in the single operation analysis (Fig. 16).

Although the analytical model does not accurately predict the optimal points at which σ_2 is minimum, as the FE and ASM2 results have similar magnitude and shape the analytical model can explain the phenomena present in the pantograph interference.

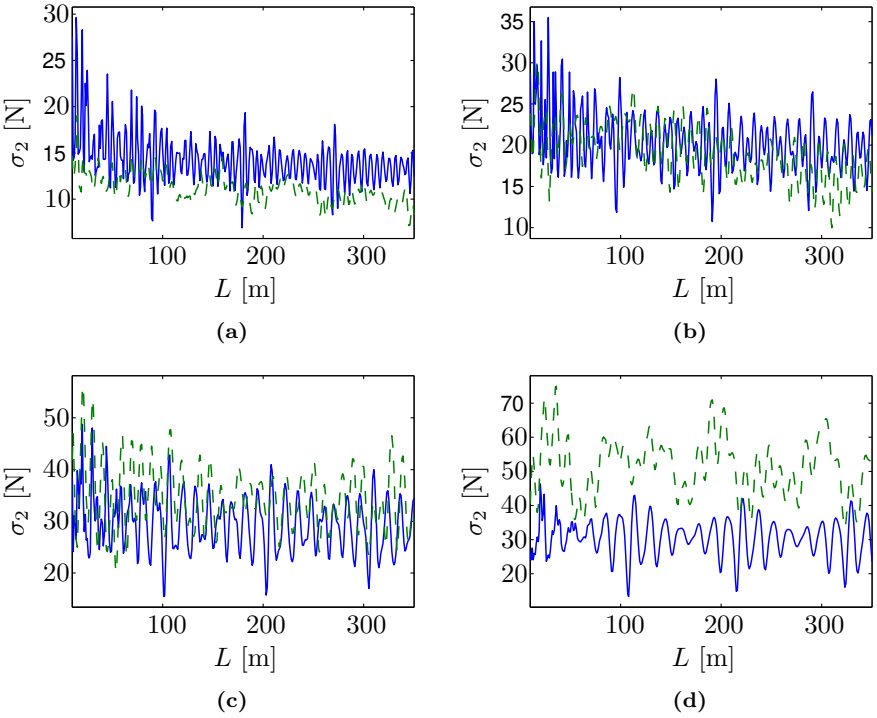

Figure 18: *SD of the trailing pantograph CF with respect to the distance between pantographs at (a) 200 km/h, (b) 250 km/h, (c) 300 km/h and (d) 350 km/h.* —— *ASM2.* – – *FEM.*

6. Conclusions

The CF variation obtained when the dynamic pantograph-catenary interaction is included in the FEM simulations is due to the combination of several sources of irregularities (geometric variation of the contact wire, stiffness and uneven mass distribution, etc.) with complex phenomena (wave propagation and reflection, complex dynamic response of the model, among others). This complexity makes these simulations computationally intensive and it is difficult to infer direct relations between the model input and output variables.

In this paper the enhanced analytical model ASM2 composed of an axially loaded infinite string with a visco-elastic support was based on that proposed in [9]. ASM2 includes a Kelvin-Voigt damping model, considers the initial height of the contact wire and uses the *penalty* method to model the contact between the pantograph and the contact wire. It also obtains an analytic expression of the steady interaction force.

Different strategies were followed to fit the ASM2 parameters in order to obtain similar behaviour to the more complex FE model. The stiffness of the support was fitted by considering a static problem, while the proper linear density of the string was obtained by considering the wavelength generated in the contact wire by harmonic excitation, and it was verified that the proposed damping model can produce the same ratio between mean dissipated power and kinetic energy to that obtained by the FE model.

The CF standard deviation σ was computed with the fitted ASM2 for a wide range of operational speeds (Fig. 16). The results obtained reveal that the initial contact wire height profile is one of the main factors that contribute to CF variation and therefore to the current collection quality. The uneven distribution of the vertical stiffness along the span is another important contribution to the CF variation, which becomes more important at high mean CF values. Since this feature is not considered in the analytical model, this can explain the greater σ obtained by the FE for the high velocities at which a greater mean CF is imposed.

A more complicated scenario arises when two pantographs interact simultaneously with the catenary, since the interference between the pantographs is a complex phenomenon which depends on wave propagation. Despite this complexity, the analytical model can separate the string response in harmonic terms and obtain a simple formula for the optimal distance between the two pantographs that gives the lowest trailing pantograph CF amplitude for every harmonic term. ASM2 thus has found the physical mechanism by which the interference occurs. In a real scenario, with a general height of the contact wire, the change of the trailing pantograph σ with respect to the distance between pantographs can be approximately predicted by the analytical model, especially at mid-range velocities.

In short, despite the simplifications and assumptions introduced, the proposed analytical model has been shown to be a basic and efficient tool for the simulation of pantograph-catenary dynamic interaction.

Acknowledgements

The authors would like to acknowledge the financial support received from the Regional Government of Valencia (PROMETEO/2016/007) and the Spanish Ministry of Economy, Industry and Competitiveness (TRA2017-84736-R), also the funds received jointly from the Regional Government of Valencia and the European Social Fund, under Grant APOSTD/2019/205.

Appendix A. Catenary and pantograph data

The values of the input parameters which define the catenary and pantograph models used in this paper are listed here. The catenary model is composed of 30 spans 65 m long. The spacing between the 7 droppers along the span is defined in Table A.3, where SA denotes the steady arm.

The mechanical and the geometric properties of the different wires of the catenary are given in Table A.4.

Table A.3: *Dropper spacing along the span.*

Droppers	SA-1	1-2	2-3	3-4	4-5	5-6	6-7	7-SA
d(m)	6	9.48	8.7	8.32	8.32	8.7	9.48	6

Table A.4: *Mechanical and geometric properties of the catenary elements.*

	ρ(kg/m^3)	E(MPa)	A(mm^2)	I(mm^4)	T (N)
Messenger wire	9114	$1.1{\cdot}10^{11}$	94.8	1237.2	15750
Contact wire	9160	$1.1{\cdot}10^{11}$	150	2170	31500
Droppers	9114	$1.1{\cdot}10^{11}$	10	0	3500 (“Y”)

The Rayleigh coefficients of the damping model are $\alpha = 0.0125$ s^{-1} and $\beta =$ 0.0001 s and the constants of the HHT integration method are $\alpha_{\text{HHT}} = -0.05$, $\beta_{\text{HHT}} = 0.2756$, $\gamma = 0.55$ and $\Delta t = 0.001$ s.

The values of the lumped parameters of the pantograph model can be seen in Table A.5. The stiffness used in the *penalty* method is $k_h = 50000$ N/m.

Table A.5: *Parameters of the pantograph model.*

d.o.f.	m(kg)	c(Ns/m)	k(N/m)
1	6.6	0	7000
2	5.8	0	14100
3	5.8	70	80

References

[1] F. Kieling, R. Puschmann, A. Schmieder, E. Schneider, Contact lines for electrical railways: Planning, Design, Implementation, Maintenance, 3rd Edition, Publicis Publishing, Erlangen, Germany, 2018.

[2] EN 50318, Railway applications. Current collection systems. Validation of simulation of the dynamic interaction between pantograph and overhead contact line, European Union Agency for Railways.

[3] S. Bruni, J. Ambrosio, A. Carnicero, Y. H. Cho, L. Finner, M. Ikeda, S. Y. Kwon, J. P. Massat, S. Stichel, M. Tur, The results of the pantograph-catenary interaction benchmark, Vehicle System Dynamics 53 (3) (2015) 412–435.

[4] M. Aboshi, K. Manabe, Analyses of contact force fluctuation between catenary and pantograph., Quarterly Report of Railway Technical Research Institute 41 (2000) 182–187.

[5] P. Nåvik, A. Rønnquist, S. Stichel, The use of dynamic response to evaluate and improve the optimization of existing soft railway catenary systems for higher speeds, Proceedings of the Institution of Mechanical Engineers, Part F: Journal of Rail and Rapid Transit 230 (4) (2016) 1388–1396.

[6] J. Pombo, J. Ambrósio, Influence of pantograph suspension characteristics on the contact quality with the catenary for high speed trains, Computers & Structures 110 (2012) 32–42.

[7] T. Wu, M. Brennan, Basic analytical study of pantograph-catenary system dynamics, Vehicle System Dynamics 30 (6) (1998) 443–456.

[8] W. Zhang, N. Zhou, R. Li, G. Mei, D. Song, Pantograph and catenary system with double pantographs for high-speed trains at 350 km/h or higher, Journal of Modern Transportation 19 (1) (2011) 7–11.

[9] S. Roy, G. Chakraborty, A. DasGupta, Coupled dynamics of a viscoelastically supported infinite string and a number of discrete mechanical systems moving with uniform speed, Journal of Sound and Vibration 415 (2018) 184 – 209.

[10] P. Belotserkovskiy, Forced oscillations and resonance of infinite periodic strings, Journal of Sound and Vibration 204 (1) (1997) 41 – 57.

[11] A. Metrikine, A. Bosch, Dynamic response of a two-level catenary to a moving load, Journal of Sound and Vibration 292 (3) (2006) 676 – 693.

[12] Z. Liu, F. Duan, Z. Xu, X. Lu, Wave propagation analysis in high-speed railway catenary system subjected to a moving pantograph, Applied mathematical modelling. 59 (2018) 20–38.

[13] M. Aboshi, M. Tsunemoto, Installation guidelines for shinkansen high speed overhead contact lines, Quarterly Report of Railway Technical Research Institute 52 (2011) 230–236.

[14] O. V. Van, J.-P. Massat, C. Laurent, E. Balmes, Introduction of variability into pantograph–catenary dynamic simulations, Vehicle System Dynamics 52 (10) (2014) 1254–1269.

[15] S. Gregori, M. Tur, J. E. Tarancón, F. J. Fuenmayor, Stochastic monte carlo simulations of the pantograph–catenary dynamic interaction to allow for uncertainties introduced during catenary installation, Vehicle System Dynamics 57 (4) (2019) 471–492.

[16] O. V. Van, J.-P. Massat, E. Balmes, Waves, modes and properties with a major impact on dynamic pantograph-catenary interaction, Journal of Sound and Vibration 402 (2017) 51 – 69.

[17] Y. H. Cho, K. Lee, Y. Park, B. Kang, K. nam Kim, Influence of contact wire pre-sag on the dynamics of pantograph–railway catenary, International Journal of Mechanical Sciences 52 (11) (2010) 1471 – 1490, special Issue on Non-linear Oscillations.

[18] S. Gregori, M. Tur, E. Nadal, F. J. Fuenmayor, An approach to geometric optimisation of railway catenaries, Vehicle System Dynamics 56 (8) (2018) 1162–1186.

[19] M. Tur, E. García, L. Baeza, F. Fuenmayor, A 3D absolute nodal coordinate finite element model to compute the initial configuration of a railway catenary, Engineering Structures 71 (2014) 234–243.

[20] S. Gregori, M. Tur, E. Nadal, J. Aguado, F. J. Fuenmayor, Chinesta, Fast simulation of the pantograph–catenary dynamic interaction, Finite Elements in Analysis and Design, 2017.

[21] Z. Liu, P.-A. Jönsson, S. Stichel, A. Rønnquist, On the implementation of an auxiliary pantograph for speed increase on existing lines, Vehicle System Dynamics 54 (8) (2016) 1077–1097.

[22] H. M. Hilber, T. J. R. Hughes, R. L. Taylor, Improved numerical dissipation for time integration algorithms in structural dynamics, Earthquake Engineering & Structural Dynamics 5 (3) (1977) 283–292.

[23] D. Anastasio, A. Fasana, L. Garibaldi, S. Marchesiello, Analytical investigation of railway overhead contact wire dynamics and comparison with experimental results, Mechanical Systems and Signal Processing 116 (2019) 277–292.

[24] EN 50367, Railway applications. Current collection systems. Technical criteria for the interaction between pantograph and overhead line, European Committee for Electrotechnical Standardization.